Preparation of Composite Particles of Bulk $Ba_2YCu_3O_{7-X}$ by Electrostatic Adhesion Process

Yasumasa Takao, Masanobu Awano, and Yoshitaka Kuwahara
National Industrial Research Institute of Nagoya, AIST, MITI, Nagoya 462, Japan

Electrostatic adhesion processes are used in preparing composite aerosol particles with the electrostatic adhesion force acting between electropositively-charged and electronegatively-charged particles. This process enables one to disperse the core and subcomponent particles more uniformly and to control the amounts of subcomponent particles adhered to the surface of individual core particles by adjusting the charging voltage. Using the composite particles prepared by the electrostatic adhesion process as a starting powder for sintering, a composite bulk body of the $Ba_2YCu_3O_{7-X}$ oxide superconductor with $BaZrO_3$ inclusions is produced. $BaZrO_3$ particles with diameters less than 100 nm are uniformly dispersed in the $Ba_2YCu_3O_{7-X}$ matrix. The composite bulk body shows improvement in critical current density, which is based on the uniform dispersion of fine $BaZrO_3$ particles as magnetic flux pinning centers. These advantages are attributed to the uniform dispersion of $BaZrO_3$ over the whole starting powder.

Introduction

Aerosol processes have been established as important techniques for preparing ultrafine particles of uniform size, morphology and high chemical purity (Okuyama et al., 1991). It has been found that an electrostatic force is effective in controlling the agglomerate structure by adjusting individual aerosol particle mobility (Matsuyama and Yamamoto, 1987). Titania-polystyrene latex composite particles have been prepared utilizing an electrostatic agglomeration (Endoh et al., 1989); however, there are few reports on composite particle preparation using an electrostatic force.

This article is concerned with the control of the amount of subcomponent particle adherence to the surface of a core aerosol particle (quantitative composite particle preparation) through the use of a bidirectional monopolar ionic charging method. Figure 1 shows an example of a subcomponent: a core particle agglomeration ratio of 1:1 and 4:1 for charging levels $-4:+4$ and $-4:+1$, respectively. In this electrostatic composite particle preparation process utilizing electrostatic adhesion, the charging polarity and rate supplied to the individual particles are controllable using compulsory ionic charging. This is possible even though the difference in the series of frictional electrification of the particles is not large. This work also studies the utilization of composite particles as a starting powder for sintering, thus ensuring the uniform dispersion of fine subcomponent particles with diameters less than 100 nm in a sintered body. In the case of an oxide superconductor, since moving magnetic flux produces an electric resistivity, magnetic flux pinning is important. A nonsuperconductive phase dispersion of flux pinning centers is effective for flux pinning enhancement. The finer the dispersion of the phase, the larger the pinning contribution and, in

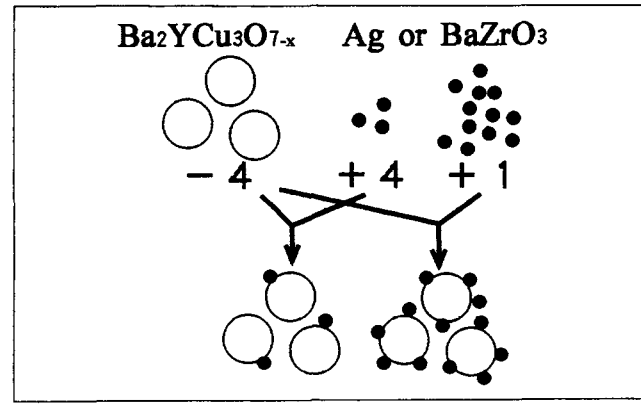

Figure 1. Quantitative composite particle prepared by the electrostatic adhesion process.

Correspondence concerning this article should be addressed to: Y. Takao, National Industrial Research Institute of Nagoya, AIST, MITI, 1-1, Hirate-cho, Kita-ku, Nagoya 462, Japan.

turn, an improved critical current density (Murakami et al., 1991). Utilization of composite powder comprised of superconductive (core) and nonsuperconductive (subcomponent) particles as a starting powder for sintering is effective in uniformly dispersing fine subcomponent particles (Takao et al., 1995). In this study, composite particles consisting of $Ba_2YCu_3O_{7-X}$ as core particles and $BaZrO_3$ as subcomponent particles (flux pinning centers) were utilized.

Experimental Setup

Scheme of electrostatic adhesion process

As shown in Figure 2, this process consists of an initial subprocess which supplies an aerosol particle by a mist pyrolysis method (aerosol generator), a second subprocess which charges the particles via a bidirectional monopolar ionic charging method (charging unit), a third subprocess which mixes the charged particles by an AC electric field (mixing unit), and a final subprocess which collects the resultants by an electrostatic precipitator (ESP). In this article, the powder collected at the ESP is termed the composite powder, and the individual agglomerated particle is termed the composite particle.

The subprocess for the generation of core and subcomponent particles uses the mist pyrolysis method. Droplets of nitrate solution produced by an ultrasonic nebulizer (vibration frequency: 1.7 MHz) were utilized. The droplets were fed with the aid of oxygen gas into each reaction zone having a 27-mm-ID, 800-mm-long heating element. The prepared particles were supplied into each charging unit with Ar gas. The gas was used to prevent the adhesion of particles to the wall of the preparation line and to produce the plasma at the charging unit by the dissociation of Ar. The charging unit is comprised of a 35-mm-ID, 70-mm-long alumina cylindrical charger (Masuda Laboratory Co.). The charger uses a bidirectional monopolar ionic charging method capable of charging up to the saturation level in a relatively short charging time. The static electricity applied to core particles and subcomponent particles were set to the opposite polarity. The charged particles were fed into a mixing unit. The mixing unit is comprised of a 50-mm-ID, 130-mm-long alumina cylinder. The mixing unit subprocess is used to increase the particle flow rate in the direction perpendicular to the main flow by using an AC electric field. Since the Coulomb effect acting between the core and subcomponent particles is amplified, subcomponent particles adhere to core particles in specific ratios, and a uniform composite particle is produced in the mixing unit. The resultant powder, consisting of individual composite particles, is collected by a DC corona discharge type electrostatic precipitator (ESP).

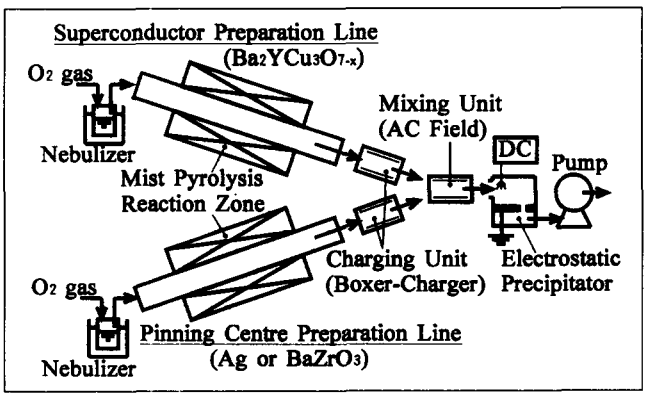

Figure 2. Experimental setup of the electrostatic adhesion process.

Experimental conditions

The core particle of yttrium oxide superconductor ($Ba_2YCu_3O_{7-X}$) was produced by using a nitrate solution with an atomic ratio of Ba:Y:Cu = 2:1:3. Ag or $BaZrO_3$ was utilized as the subcomponent particle. Ag was produced by using a nitrate solution of dissolved Ag_2O. The $Ba_2YCu_3O_{7-X}$-Ag composite particle was used to verify the contribution of the electrostatic force for dispersing and mixing the individual particles more uniformly. Since Ag particles are easily distinguishable from $Ba_2YCu_3O_{7-X}$ in scanning electron microscope (SEM) observation at low magnification, the distribution status of each particle is easily confirmed over the whole of the composite powder. The concentration of nitrate solution and the carrier gas flow rate were set to 0.05 mol/L, 1 L/min, for $Ba_2YCu_3O_{7-X}$ and 0.04 mol/L, 3 L/min for Ag. The $BaZrO_3$ subcomponent particle was produced by using a nitrate solution into which a zirconia sol was added for a chemical composition of Ba:Zr = 1:1. The $Ba_2YCu_3O_{7-X}$-$BaZrO_3$ composite particle was used to verify the level to which $BaZrO_3$ adhered to a $Ba_2YCu_3O_{7-X}$ particles, and to confirm the improved characteristics of the sintered body produced from the composite powder. The concentration of nitrate solution and the carrier gas flow rate were set to 0.1 mol/L, 1.5 L/min for $Ba_2YCu_3O_{7-X}$ and 0.0005 mol/L, 4.5 L/min for $BaZrO_3$. Feedstreams of core and subcomponent particles were kept at 950°C.

Both Ar gas flow rates for core and subcomponent particles were set to 1 L/min to prevent particle adhesion and to produce plasma by Ar dissociation. Charging voltages for each particle were adjusted between 0 kV and 20 kV/500 Hz at a constant excitation voltage of 5 kV/20 kHz. The static electricity applied to the $Ba_2YCu_3O_{7-X}$ core particle was negative, while that applied to the subcomponent particles (Ag or $BaZrO_3$) was positive. The AC field of the mixing unit was set to 20 kV/200 Hz. The ESP used a disc (SUS304) of 150 mm in diameter and a 10 kV DC corona discharge.

Collected powder was shaped to the size of 20 mm × 3 mm × 1 mm by uniaxial pressing, and pressed by cold isostatic pressing at 200 MPa. The compact body was sintered at 900 ~ 910°C for 30 h, and then annealed in an oxygen flow at 500°C for 40 h.

Evaluation

The collected powder at the ESP was evaluated by X-ray diffraction analysis (XRD), SEM observation, and analytical electron microscopy (AEM). The contribution of electrostatic force for uniformly dispersing the individual particles was verified by SEM analysis of the $Ba_2YCu_3O_{7-X}$-Ag composite particle. Quantitative control of subcomponent particle adherence onto a core particle was verified by AEM analysis of $Ba_2YCu_3O_{7-X}$-$BaZrO_3$ composite particles. Polished surfaces of sintered bodies were observed by SEM and electron probe microanalysis (EPMA). Zr concentration was evaluated with inductively coupled plasma emission spectroscopy (ICP) of

$Ba_2YCu_3O_{7-X}$-$BaZrO_3$ composite powder. The temperature dependence of electrical resistivity was measured by a DC four-probe method with a current of 10 mA, and the transport critical current density (J_{ct}) was evaluated by a DC four-probe method with a criterion of 1 μV/cm at 77 K in OT (Mizutani et al., 1989). The magnetic hysteresis loops were measured with superconductive quantum interference device magnetometer (SQUID). The onset critical temperature ($T_{c(onset)}$) was confirmed by the temperature dependence of magnetization. The end point of critical temperature ($T_{c(end)}$) was measured from the temperature dependence of resistivity. The intragrain (magnetic) critical current density (J_{cm}) was determined using the assumption of the Bean critical state model, that is, $J_{cm} = 20\Delta$ M/d. The width of the magnetic hysteresis loops (ΔM, emu/cm^3) were obtained from the loops by increasing and decreasing magnetic field at an appropriate temperature. The average grain size was determined as the appropriate length (d, cm) derived from the Bean model (Mizutani et al., 1989). The grain size was obtained from SEM photograph.

Results and Discussion

Composite particle

Figure 3 shows how the composite status varies in response to a change in the charging voltage when core particles and subcomponent particles are mixed. These are SEM photographs of the $Ba_2YCu_3O_{7-X}$-Ag composite powder collected at the ESP. Figure 3a shows the composite status for the mixing of uncharged $Ba_2YCu_3O_{7-X}$ and Ag particles. Figure 3b shows the case for both $Ba_2YCu_3O_{7-X}$ and Ag particles charged to 5 kV. Figures 3c and 3d show the case for both particles charged to 20 kV. As is clearly shown in Figure 3a, both uncharged $Ba_2YCu_3O_{7-X}$ particles (large, gray) and unchanged Ag particles (small, white) show nonuniform agglomeration. As can be seen in Figures 3b and 3c, agglomeration is eliminated by charging the particles and increasing the charging voltage. Figure 3c indicates that both $Ba_2YCu_3O_{7-X}$ and Ag particles are uniformly mixed. Figure 3d shows the photograph of the powder in Figure 3c at high magnification. $Ba_2YCu_3O_{7-X}$-Ag composite particles in which Ag particles are adhered onto the surface of a $Ba_2YCu_3O_{7-X}$ particle were then prepared. This improvement of the distribution status of each particle is likely based on the electrostatic repulsion between particles charged to the same polarity, and the electrostatic agglomeration between particles charged to opposite polarity.

Figure 4 shows how the adhesion of subcomponent particles varies in response to the change in the charging ratio of core and subcomponent particles. Figure 4a shows the transmission electron microscope (TEM) photograph of a $Ba_2YCu_3O_{7-X}$-$BaZrO_3$ composite particle prepared at the

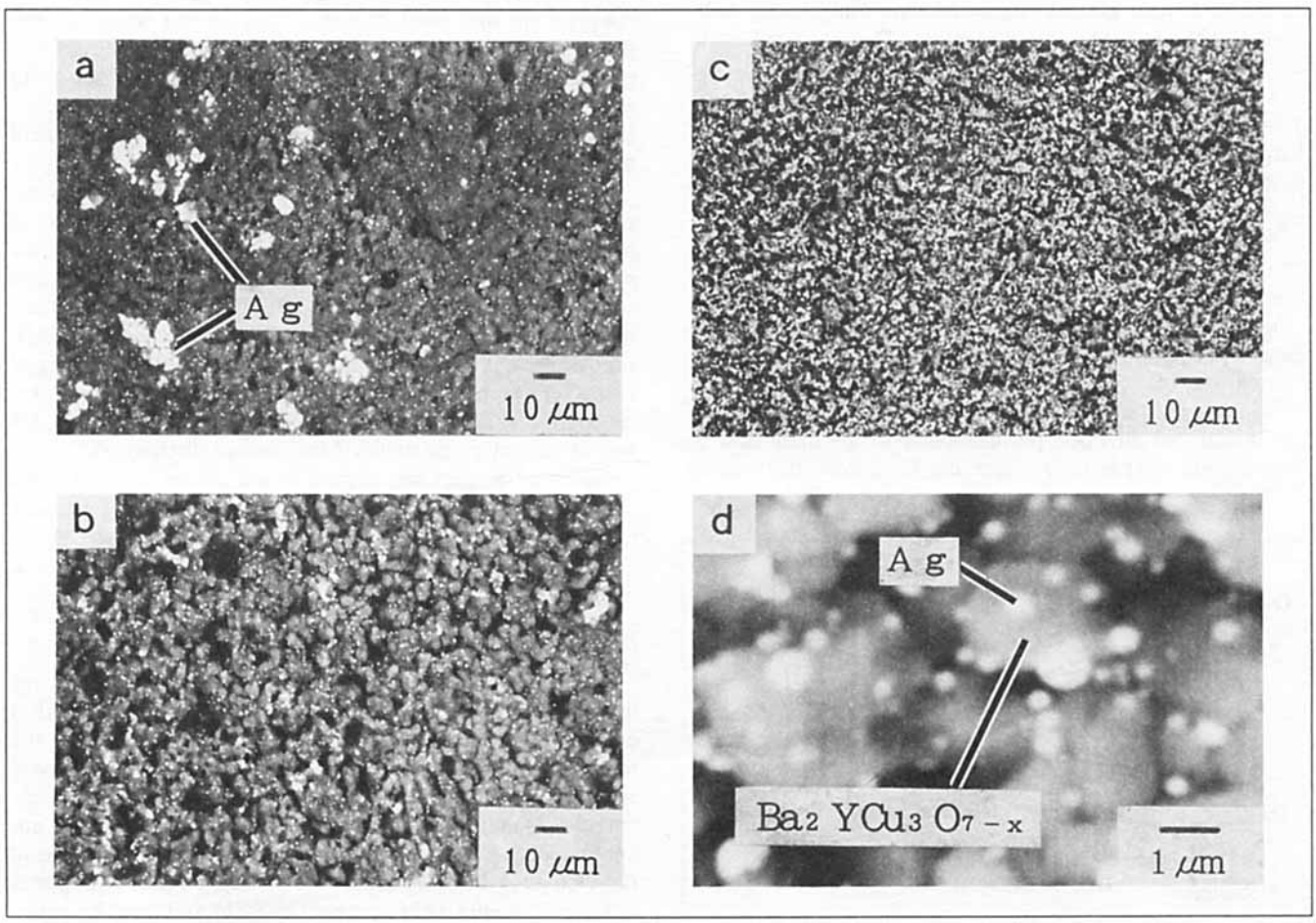

Figure 3. Scanning electron micrographs of $Ba_2YCu_3O_{7-x}$-Ag composite particles.

(a) Uncharged; (b) $Ba_2YCu_3O_{7-X}$ = 5 kV, Ag = 5 kV; (c) and (d) $Ba_2YCu_3O_{7-X}$ = 20 kV, Ag = 20 kV.

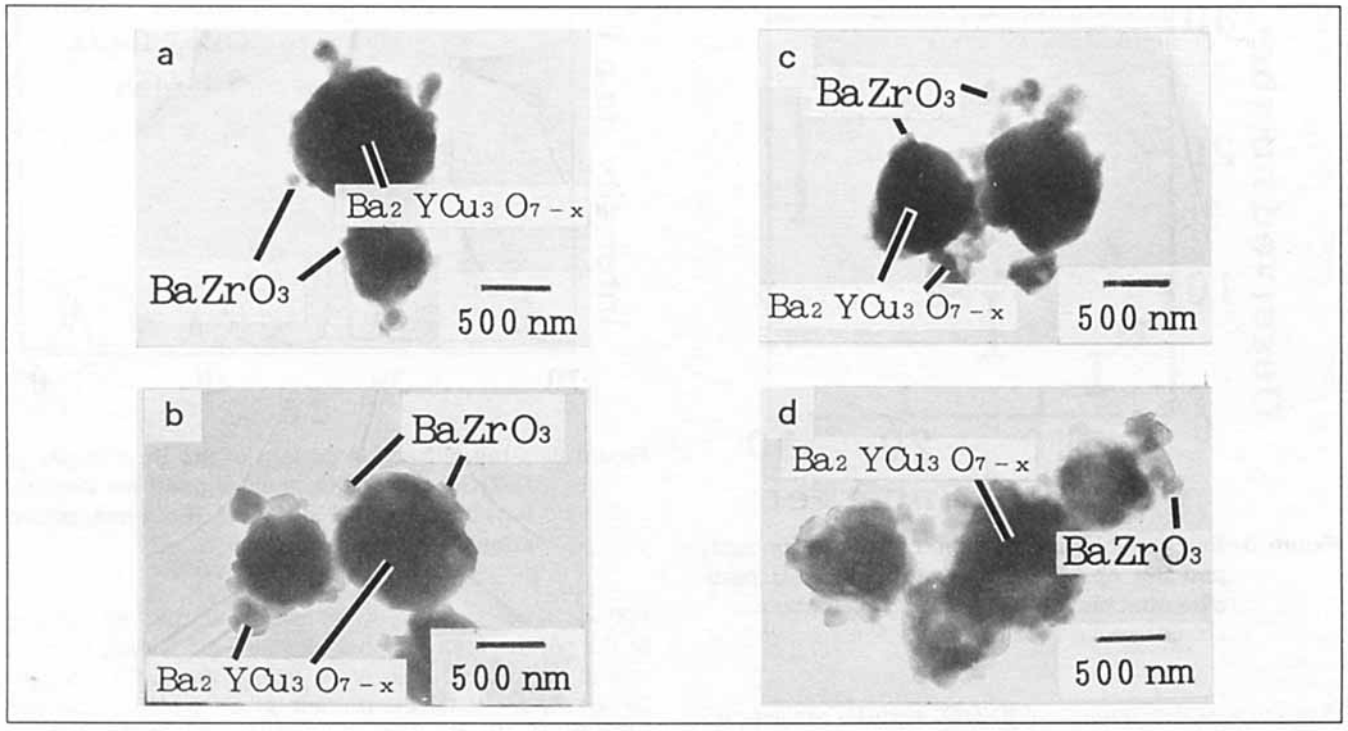

Figure 4. Transmission electron micrographs of $Ba_2YCu_3O_{7-X}$-$BaZrO_3$ composite particles.

(a) $Ba_2YCu_3O_{7-X}$ = 10 kV, $BaZrO_3$ = 20 kV; (b) $Ba_2YCu_3O_{7-X}$ = 20 kV, $BaZrO_3$ = 20 kV; (c) $Ba_2YCu_3O_{7-X}$ = 20 kV, $BaZrO_3$ = 15 kV; (d) $Ba_2YCu_3O_{7-X}$ = 20 kV, $BaZrO_3$ = 10 kV.

charging voltage condition of 10 kV for $Ba_2YCu_3O_{7-X}$ and 20 kV for $BaZrO_3$. Under this condition, the charging ratio of $BaZrO_3$ to $Ba_2YCu_3O_{7-X}$ is 7. Note that the charging ratio was obtained from the charge imparted to $BaZrO_3(q_z)$ and that of $Ba_2YCu_3O_{7-X}(q_y)$ as q_z/q_y. Figure 1 shows an example of $BaZrO_3$:$Ba_2YCu_3O_{7-X}$ charge of $-4:+4$ and $-4:+1$. The charging ratio of $-4:+4$ is 1 and that of $-4:+1$ is 4. Besides, the charge imparted to each particle was calculated by using the assumption that each particle was charged to its maximum level (saturation level) due to field charging (Masuda et al., 1991). This assumption is justifiable in this experiment, because the particle flow rate was set at a condition such that particles were retained in the charging zone for a longer time than that required for complete saturation. Figure 4b shows results for a 20 kV charge for $Ba_2YCu_3O_{7-X}$ and a 20 kV charge for $BaZrO_3$ (charging ratio is 14). Figure 4c shows results for a charge of 20 kV for $Ba_2YCu_3O_{7-X}$ and 15 kV for $BaZrO_3$ (charging ratio = 19). Figure 4d shows results for a charge of 20 kV for $Ba_2YCu_3O_{7-X}$ and 10 kV for $BaZrO_3$ (charging ratio = 28). Figure 4 shows that $BaZrO_3$ particles with diameters less than 100 nm adhere onto a $Ba_2YCu_3O_{7-X}$ core particle of less than 1 μm diameter. Adhesion levels of $BaZrO_3$ particles increased according to the increase in the charging level. To further investigate the tendency of the adhered level to increase with the charging ratio, the observed amount of $BaZrO_3$ obtained from experimental results (as shown in Figure 4) was compared with the charging ratio of $BaZrO_3$ to $Ba_2YCu_3O_{7-X}$. The observed amount of $BaZrO_3$ particles adhering to a $Ba_2YCu_3O_{7-X}$ core particle was obtained by counting the $BaZrO_3$ particles in the TEM photographs. $BaZrO_3$ particles were observed over the whole surface of a $Ba_2YCu_3O_{7-X}$ particle. In this evaluation, the $BaZrO_3$ particles were identified by the spectrum detected with energy dispersive X-ray spectroscopy (EDS). An example of an energy dispersive X-ray spectrum detected in core and subcomponent particles is shown in Figure 5. Figure 5a is the spectrum detected around the core particle ($Ba_2YCu_3O_{7-X}$), and Figure 5b is the spectrum detected around the subcomponent particle ($BaZrO_3$). Figure 6 indicates the relationship of the observed amount of $BaZrO_3$ particles adhered onto a $Ba_2YCu_3O_{7-X}$ core particle and the calculated amount which corresponds to the charging ratio of $BaZrO_3$ to $Ba_2YCu_3O_{7-X}$. As can be seen in Figure 6, the

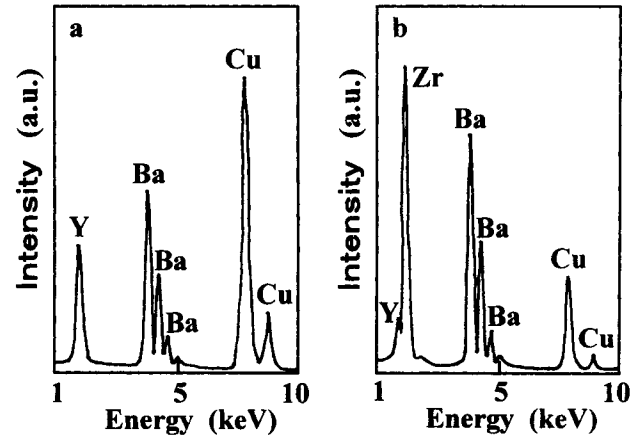

Figure 5. EDS profiles detected in $Ba_2YCu_3O_{7-X}$-$BaZrO_3$ composite particles.

(a) Profile detected around the core particle ($Ba_2YCu_3O_{7-X}$); (b) profile detected around the subcomponent particle ($BaZrO_3$).

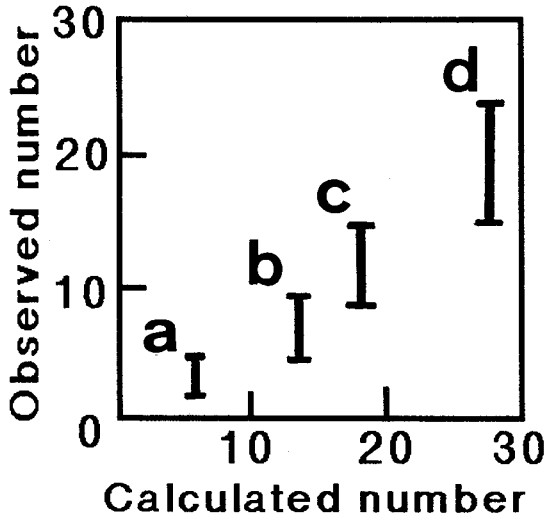

Figure 6. Relationship between the calculated amounts and the observed amounts of $BaZrO_3$ particles attached on a $Ba_2YCu_3O_{7-x}$ particle.

a-d correspond to Figures 3a-3d.

observed adhesion amounts of $BaZrO_3$ particles are approximately proportional to the calculated ones. This result reveals that the electrostatic adhesion process is capable of a quantitative control of subcomponent particles adhered onto a core particle.

Sintered body characteristics

Figure 7 shows how the microstructure of the composite bulk body varies in response to charging and uncharging. Figure 7a shows a SEM photograph of a polished surface of $Ba_2YCu_3O_{7-X}$-$BaZrO_3$ composite sintered body prepared from $Ba_2YCu_3O_{7-X}$-$BaZrO_3$ composite powder obtained by mixing uncharged $Ba_2YCu_3O_{7-X}$ particles and uncharged $BaZrO_3$ ones. Figure 7b is a result of a sintered body of $Ba_2YCu_3O_{7-X}$-$BaZrO_3$ composite powder obtained by the electrostatic adhesion process. Charging conditions for the powder corresponds to those of Figure 4d. Sintering conditions for both composite sintered bodies was 900°C for 30 h. The Zr addition ratio in comparison to Y detected by the

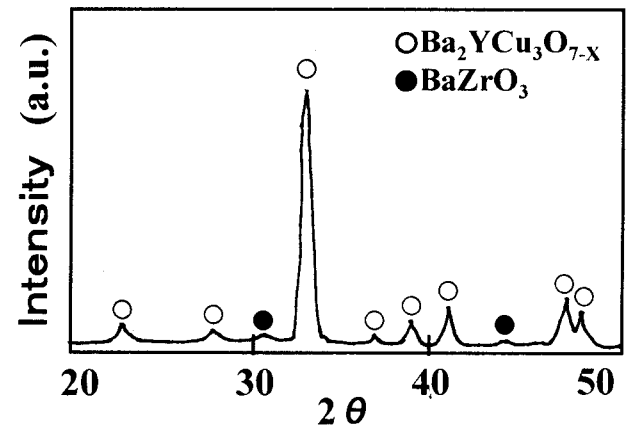

Figure 8. X-ray diffraction pattern of the $Ba_2YCu_3O_{7-X}$-$BaZrO_3$ composite powder used for producing the sintered body of the electrostatic adhesion process.

ICP was about 1 mol %. As an example of the XRD pattern of the powder used for producing sintered bodies, the pattern of the sintered body of $Ba_2YCu_3O_{7-X}$-$BaZrO_3$ composite powder due to the electrostatic adhesion process is shown in Figure 8. As shown in Figure 7a, the sintered body prepared from the uncharged powder indicates an increase of $BaZrO_3$ particle diameters and pore sizes as compared with Figure 7b. Figure 7b shows that the sintered body prepared from the powder obtained by the electrostatic adhesion process has a uniform dispersion of fine $BaZrO_3$ particles with diameters less than 100 nm, and relatively small pore sizes. This uniformity in the dispersion of subcomponent particles in the sintered body obtained by the electrostatic adhesion process is attributed to the uniform dispersion of $BaZrO_3$ over the whole of the $Ba_2YCu_3O_{7-X}$-$BaZrO_3$ composite powder (as shown in Figure 3).

Furthermore, in the case of a conventional preparation method such as the solid state method (Oka et al., 1992), the Zr added contribution is effective only after an addition of more than 10 mol %. In the case of the electrostatic adhesion process, the J_c improvement was obtained by 1 mol % Zr addition. This substantial improvement of subcomponent inclusions is attributed to the uniform dispersion of the sub-

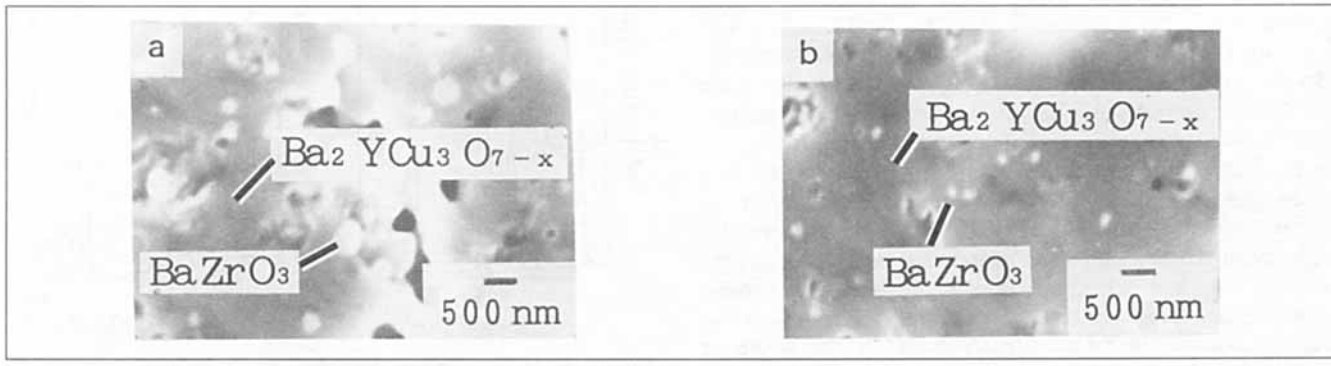

Figure 7. Scanning electron micrographs of a polished surface of $Ba_2YCu_3O_{7-X}$-$BaZrO_3$ composite sintered bodies prepared from $Ba_2YCu_3O_{7-X}$-$BaZrO_3$ composite powders.

(a) Sintered body obtained by mixing uncharged $Ba_2YCu_3O_{7-X}$ particles and uncharged $BaZrO_3$ ones; (b) sintered body of $Ba_2YCu_3O_{7-X}$-$BaZrO_3$ composite powder obtained by the electrostatic adhesion process.

component particle in the composite powder and the composite sintered body prepared by the electrostatic adhesion process. Additionally, since the powder prepared by the electrostatic adhesion process was comprised of fine particles produced by the mist pyrolysis method, the sinterability is good (Awano et al., 1992) in comparison to the conventional method. The $Ba_2YCu_3O_{7-X}$ sintered body having a 90 K critical temperature was obtained by sintering at comparatively low temperatures such as 900°C. Thus, further improvement in J_c is expected by optimizing the Zr addition ratio and the sintering conditions.

Critical current density

The magnetic properties of the $Ba_2YCu_3O_{7-X}$-$BaZrO_3$ composite sintered body and the $Ba_2YCu_3O_{7-X}$ monolithic sintered body were compared to investigate the contribution of intragrain $BaZrO_3$ particles to flux pinning. For comparing the magnetic properties of each sample, it is necessary to set at the condition of the nearly same total amount of the flux penetrated through the grain boundary when the magnetic field is applied. It is also required to equalize the temperature difference of $T_{c(end)}$ and evaluation temperature. As the standard of above conditions, $T_{c(end)}$ of each sample was unified to the same value (about 90 K) by regulating sintering temperature. Consequently, the values of $T_{c(end)}$ of $Ba_2YCu_3O_{7-X}$-$BaZrO_3$ composite bodies sintered at 900°C (shown in Figure 7) were in approximate agreement with the value of $Ba_2YCu_3O_{7-X}$ monolithic body sintered at 910°C. Thus, these sintered bodies were chosen as the sample for comparing each property. In addition, the sintering temperature of the $Ba_2YCu_3O_{7-X}$-$BaZrO_3$ composite sintered body is lower than that of monolithic body for obtaining same $T_{c(end)}$. This was caused by the decrease of the melting point of $Ba_2YCu_3O_{7-X}$ with Zr inclusions, as discussed in the previous article (Takao et al., 1994).

Figure 9 describes the magnetic field dependence of the intragrain critical current density (J_{cm}) at 77 K for the $Ba_2YCu_3O_{7-X}$-$BaZrO_3$ composite sintered bodies (charged, uncharged) and a $Ba_2YCu_3O_{7-X}$ monolithic sintered body (monolith). "Uncharged" corresponds to J_{cm} values of the composite sintered body as indicated in Figure 7a. "Charged" corresponds to J_{cm} values of the sintered body via the electrostatic adhesion process as indicated in Figure 7b. "Monolith" corresponds to J_{cm} values of the sintered body prepared from a $Ba_2YCu_3O_{7-X}$ monolithic powder produced by the mist pyrolysis method. Experimental conditions for the monolithic powder (such as a concentration of nitrate solution and a carrier gas flow rate) were the same as that for the composite powder (0.1 mol/L, 1.5 L/min).

Figure 9 shows that the both composite sintered bodies (uncharged, charged) have high J_{cm} values as compared with the $Ba_2YCu_3O_{7-X}$ monolithic sintered body (monolith). Both composite sintered bodies were sintered at 900°C and the monolithic sintered body was 910°C. Thus, the grains of the $Ba_2YCu_3O_{7-X}$ monolithic sintered body were of large size compared with those of the composite sintered bodies, such as the 3 μm of the monolith, the 1.8 μm of the uncharged, and the 1.7 μm of the charged. This result indicates that the amount of grain surface area of both composite sintered bodies are increased compared with the monolithic sintered body.

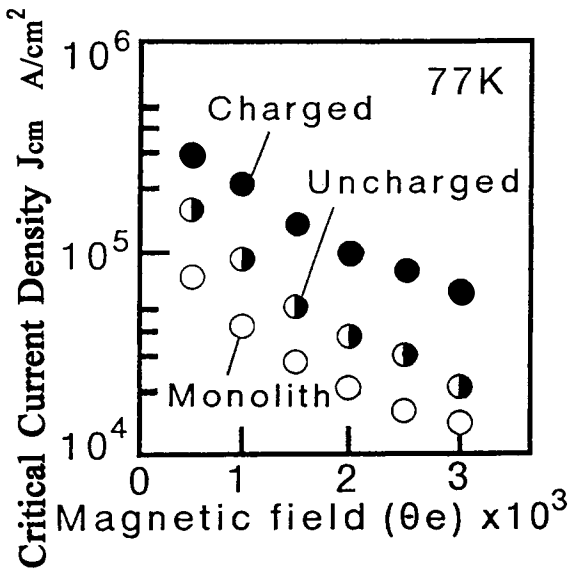

Figure 9. Magnetic field dependence of intragrain critical current density (J_{cm}) at 77 K of $Ba_2YCu_3O_{7-X}$-$BaZrO_3$ composite sintered bodies (charged, uncharged) and a $Ba_2YCu_3O_{7-X}$ monolithic sintered body (monolith).

Uncharged corresponds to the J_{cm} values of the composite sintered body indicated in Figure 6a; charged corresponds to the J_{cm} values of the sintered body via the electrostatic adhesion process indicated in Figure 6b; monolith corresponds to J_{cm} values of the sintered body made from a $Ba_2YCu_3O_{7-X}$ monolithic powder produced by a mist pyrolysis method.

However, the maximum transport critical current density J_{ct} of the monolith was 35 A/cm^2 at 77 K in 0 T, and J_{ct} of charged was 230 A/cm^2. These results show that $BaZrO_3$ particles contribute to flux pinning in the $Ba_2YCu_3O_{7-X}$ matrix as flux pinning centers.

Furthermore, Figure 9 indicates that J_{cm} values of the electrostatic adhesion process (charged) are higher in comparison with those of the composite sintered body prepared from the uncharged powder (uncharged). This corresponds to the microstructure observations shown in Figure 7. The $Ba_2YCu_3O_{7-X}$-$BaZrO_3$ composite sintered body of the electrostatic adhesion process has uniformly and finely distributed $BaZrO_3$ particles. This result corresponds to the increase of the total effective surface area of magnetic flux pinning centers. This increase results in flux pinning enhancement which leads to improvement in J_{cm}. Consequently, the use of composite particles prepared by the electrostatic adhesion process as a starting powder for sintering ensured the uniform dispersion of fine subcomponent particles with diameters less than 100 nm in the sintered body, and enabled the improvement of properties of the sintered body.

Temperature dependence of intragrain critical current density

The temperature dependence of intragrain critical current density J_{cm} was evaluated for supplementing the contribution of $BaZrO_3$ particles to flux pinning, as discussed in the

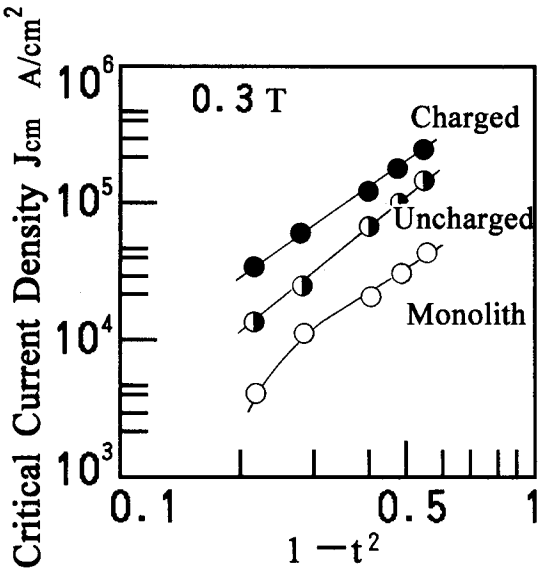

Figure 10. Temperature (T) dependence of the intragrain critical current density (J_{cm}) of $Ba_2YCu_3O_{7-X}$-$BaZrO_3$ composite sintered bodies (charged, uncharged) and a $Ba_2YCu_3O_{7-X}$ monolithic sintered body (monolith).

t is T/T_c, T_c is critical temperature.

previous report (Takao et al., 1994). Assuming a function of large nonsuperconducting particles as a magnetic flux pinning center, an empirical temperature dependence of critical current density under a fixed magnetic field is yielded as $J_c \propto 1-t^2$ on $Ba_2YCu_3O_{7-X}$, where t is T/T_c, T is temperature, and T_c is critical temperature. The large nonsuperconducting particles (such as BaY_2CuO_5 particles) are reported to be effective to enhance the flux pinning at high temperature, that is, $T > 60$ K (Matsushita et al., 1991). Using this empirical temperature dependence above 60 K, it can be checked by the contribution to flux pinning of nonsuperconducting particles distributed in the matrix, such as $BaZrO_3$. In this evaluation, T_c was expressed by $T_{c(\text{onset})}$ read from the temperature dependence of magnetization, and J_c was expressed by J_{cm}.

As illustrated in Figure 10, the temperature dependence of J_{cm} of both the $Ba_2YCu_3O_{7-X}$-$BaZrO_3$ composite sintered bodies (uncharged, charged) show the reasonable agreement with $J_c \propto 1-t^2$, while J_{cm} of $Ba_2YCu_3O_{7-X}$ monolithic sintered body (monolith) drops more quickly with temperature. These results also show that $BaZrO_3$ particles distributed in the composite sintered bodies contribute to flux pinning, and the electrostatic adhesion process ensures that contribution.

Magnetic hysteresis loops of crushed powder

As discussed in Figure 9, the average grain size was different from $Ba_2YCu_3O_{7-X}$-$BaZrO_3$ composite sintered bodies and a monolithic body. In this case, there might be uncertainties due to the difference of the total amount of flux penetrated through the grain boundary when the magnetic field was applied. To eliminate uncertainties due to the size, the comparison of the magnetic hysteresis loops were obtained on the finely crushed powders of each sintered body, the average size of which was smaller than the average grain size of the sintered body (Sengupta et al., 1992). Therefore, since the crushed powders had similar particle sizes, direct comparisons could be made between the intragrain flux pinning effects of composite and monolithic sintered bodies.

Figure 11 shows SEM photographs of the powders. Figure 11a shows the crushed powder of the $Ba_2YCu_3O_{7-X}$ monolithic sintered body indicated in Figures 9 and 10 as monolith. Figure 11b is the $Ba_2YCu_3O_{7-X}$-$BaZrO_3$ composite sintered body shown in Figures 7a, 9, and 10 as uncharged, and Figure 11c is also composite body shown in Figures 7b, 9 and 10 as charged. Each crushed powder has similar particle sizes.

Figure 12 shows magnetic hysteresis loops of each crushed powder. The area of hysteresis loop of charged increase compared to uncharged and monolith. Since the results constitute direct evidence for the benefits to flux pinning of intragrain pinning effects, Figure 12 supports the conclusion that the $BaZrO_3$ particles introduce the flux pinning centers into the grain, and the use of the electrostatic adhesion process enables the contribution to the flux pinning of the intragrain pinning effects. Consequently, Figures 9, 10 and 12 indicate that the electrostatic adhesion process is effective to introduce $BaZrO_3$ particles as flux pinning centers.

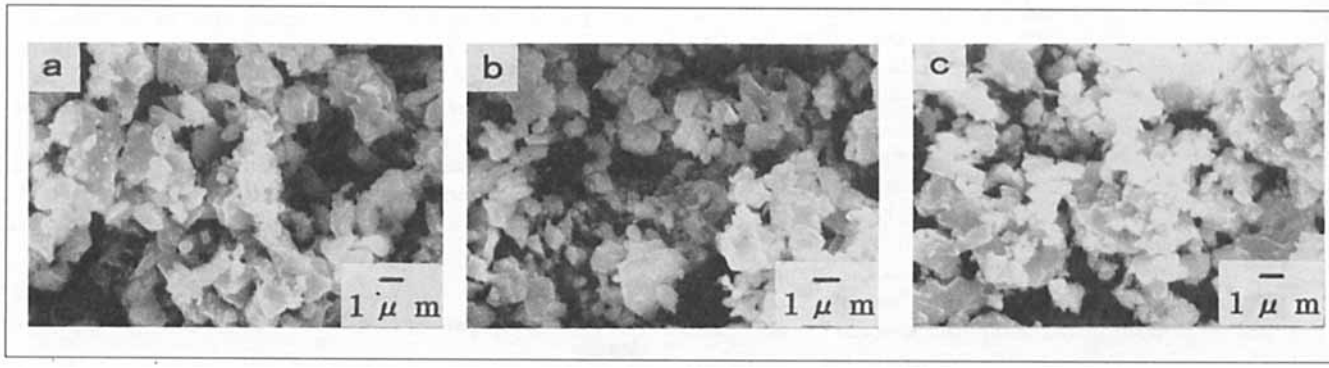

Figure 11. SEMs of crushed powders of $Ba_2YCu_3O_{7-X}$-$BaZrO_3$ composite sintered bodies (charged, uncharged) and a $Ba_2YCu_3O_{7-X}$ monolithic sintered body (monolith).

(a) Monolith; (b) uncharged; (c) charged.

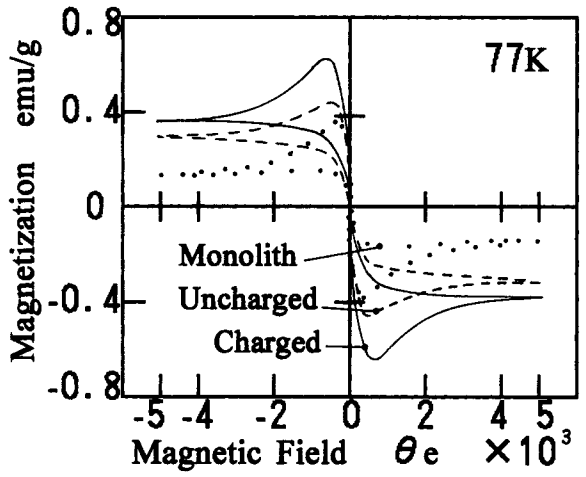

Figure 12. Magnetic hysteresis loops of crushed powders of $Ba_2YCu_3O_{7-X}$-$BaZrO_3$ composite sintered bodies (charged, uncharged) and a $Ba_2YCu_3O_{7-X}$ monolithic sintered body (monolith).

Conclusions

(1) The electrostatic adhesion process enabled core ($Ba_2YCu_3O_{7-X}$) and subcomponent ($BaZrO_3$) particles to be dispersed more uniformly, and allowed for the control of the amount of subcomponent particles adhering to the surface of a core particle by adjusting the charging voltage.

(2) Sintered bodies made from composite powder produced by the electrostatic adhesion process showed a uniform dispersion of fine subcomponent particles ($BaZrO_3$) with diameters less than.100 nm.

(3) Transport and intragrain critical current density of the $Ba_2YCu_3O_{7-X}$-$BaZrO_3$ sintered body prepared by the electrostatic adhesion process increased in comparison to the monolithic $Ba_2YCu_3O_{7-X}$. The temperature dependence of critical current density of the composite was yielded as $J_c \propto 1 - (T/T_c)^2$, and the area of magnetic hysteresis loops of the crushed powder also increased. It was clarified that the electrostatic adhesion process was effective for the introduction of $BaZrO_3$ particles as flux pinning centers.

Acknowledgment

The authors would like to acknowledge the guidance and advice of Professor Hideo Yamamoto of the Soka University for the fabrication of experimental equipment and Dr. David P. Brown of the University of Cincinnati in the preparation of the manuscript.

Literature Cited

Awano, M., Y. Takao, K. Kani, and H. Takagi, "Synthesis and Properties of Powdered Oxide Superconductor by the Mist Pyrolysis Method," *J. Chem. Eng. Jpn.*, **25**, 508 (1992).

Endoh, S., K. Okuda, J. Koga, S. Matsumoto, and K. Takeuchi, "Synthesis of Composite Fine Particles in the Gas Phase," *J. Soc. Powder Technol. Jpn.*, **26**, 174 (1989).

Masuda, S., M. Washizu, and T. Ohtani, "BOXER-CHARGER—A Bi-Directional Monopolar Charging Device," *Proc. World Cong. Powder Technol.*, Part 1, G. Jimbo, K. Leschonski, and K. Beddow, eds., Soc. of Powder Technol., Japan, Kyoto, p. 313 (1991).

Matsushita, T., E. Otabe, B. Ni, K. Kimura, M. Morita, M. Tanaka, M. Kimura, K. Miyamoto, and K. Sawano, "Critical Current Characteristics in Superconducting Y-Ba-Cu-O prepared by the Melt Process," *Jpn. J. Appl. Phys.*, **30**, L342 (1991).

Matsuyama, T., and H. Yamamoto, "Charge Transfer between a Single Polymer Particle and a Metal Plate due to Impact," *J. Soc. Powder Technol. Jpn.*, **24**, 765 (1987).

Mizutani, N., A. Nanjo, K. Shinozaki, M. Kato, and H. Masuda, "Effects of Microstructure on the Critical Current Density of Superconducting $YBa_2Cu_3O_X$," *J. Ceram. Soc. Jpn.*, **97**, 1021 (1989).

Murakami, M., H. Fujimoto, S. Gotoh, K. Yamaguchi, N. Koshizuka, and S. Tanaka, "Flux Pinning due to Nonsuperconducting Particles in Melt Processed YaBaCuO Superconductors," *Physica C*, **185–189**, 321 (1991).

Oka, T., Y. Itoh, Y. Yanagi, H. Tanaka, S. Takashima, and U. Mizutani, "Metallurgical Reactions and Their Relationships to Enhanced Mechanical Strength in Zr-Bearing YBCO Composite Superconductors," *Jpn. J. Appl. Phys.*, **31**, L1760 (1992).

Okuyama, K., K. Ohshima, and K. Tsuto, "Preparation of Micro Controlled Particles using Aerosol Process Technology," *KONA*, **9**, 79 (1991).

Sengupta, S., D. Shi, Z. Wang, A. Biondo, U. Balachandran, and K. Goretta, "Effect of Y_2BaCuO_x Precipitates on Flux Pinning in Melt-Processed $YBa_2Cu_3O_x$," *Physica C*, **199**, 43 (1992).

Takao, Y., M. Awano, and H. Takagi, "Preparation and Properties of $Ba_2YCu_3O_{7-X}$-$BaZrO_3$ Superconductive Composite by Spray Drying Method," *J. Ceram. Soc. Jpn.*, **102**, 237 (1994).

Takao, Y., M. Awano, K. Kuwahara, and Y. Murase, "Preparation of a Oxide Superconductive Composite using Aerosol Process Technology," *J. Soc. Powder Technol. Jpn.*, **32**, 144 (1995).

Manuscript received Oct. 28, 1996, and revision received May 5, 1997.